Chiral dynamics in QCD at finite chemical potential

Sourendu Gupta* and R. Ray†

Department of Theoretical Physics, Tata Institute of Fundamental Research, Homi Bhabha Road, Mumbai 400005, India
(Received 26 September 2004; published 9 December 2004)

We present the renormalized Taylor expansion of the chiral condensate with chemical potential. The relation with the Taylor coefficients of meson susceptibilities and the quark mass dependence of the quark number susceptibilities are obtained through chiral Ward identities and Maxwell relations. The continuum limit is obtained in quenched and two flavor QCD. In $N_f = 2$ QCD, the quadratic response coefficients of the chiral condensate to chemical potential indicate that pion fluctuations decrease at finite chemical potential toward the critical end point. We discuss how these observables can be used to test other features of the QCD phase diagram.

I. INTRODUCTION

Studies of hot dense matter formed in heavy-ion colliders such as the RHIC [1] need to be interpreted using theoretical predictions obtained from lattice computations. Most of these are performed at zero baryon density. However, it seems likely that the actual experimental conditions involve small but nonvanishing baryon chemical potential. In order to deal with this one has to consider the stability of various lattice predictions to the presence of a small chemical potential, μ.

This was once considered an insoluble problem in lattice QCD. The reason is that direct lattice Monte Carlo simulations at finite μ are impossible since the weights in the partition function are not positive definite. However, developments in recent years [2–5] mean that QCD at finite μ is no longer out of reach on the lattice. In this paper we investigate Taylor expansions in the chemical potential [4,6,7], which have recently been used to compute the equation of state at finite μ [4,5].

The first investigations of correlators at finite chemical potential were performed in [7]. Our approach differs from theirs in that we do a direct Taylor expansion of operators, rather than of parameters in fitting functions. There is a conceptual and practical gain. Putting chemical potentials on quarks can break the flavor $\times$ CP symmetry of QCD in many different ways, possibly affecting every observable in distinct fashion. However it turns out that there are enough relations between operators and their derivatives that, among all the observables related to chiral dynamics in QCD, there is only one set of independent Taylor coefficients. Taylor expansions of the operators utilize these relations with generality and economy.

There turn out to be three independent parameters of interest in the chiral sector—a single linear response coefficient of the chiral condensate to μ, and two quadratic response coefficients (QRCs). The linear coefficient

vanishes by symmetry in an expansion around $\mu = 0$. Thus, the two chiral QRCs encapsulate the physics arising from the influence of baryon dynamics due to $\mu \neq 0$ on chiral fluctuations. Since the phase diagram of QCD at small μ is built up through the interplay of chiral and baryon dynamics [8–11], the QRCs provide direct information on this phase diagram.

Here we present the first systematic study of the renormalized Taylor expansion of the chiral condensate in QCD up to second order in the chemical potentials [12]. We define renormalization schemes which are simple to implement, and in which the Taylor expansion can be extrapolated to the continuum. We find the continuum limits at both high and low temperatures in quenched and dynamical $N_f = 2$ QCD.

In Sec. II we write out generic Taylor expansions in the chemical potential, before specializing to pure glue operators, the chiral condensate, and meson susceptibilities. The renormalization schemes for the condensate, Maxwell relations, and chiral Ward identities are also dealt with in this section. The actual lattice simulations and results are in Sec. III, including the complete specification of the renormalization schemes and results above and below T_c in the quenched theory. This section also contains our results for QCD with dynamical quarks. Discussion of the results and the constraints that the QRCs can place on the QCD phase diagram can be found in the concluding Sec. IV.

II. TAYLOR EXPANSIONS

The partition function of QCD at temperature T and chemical potentials μ_f for each flavor f of quarks is

$$Z(\{m_f\}, T, \{\mu_f\}) = \int \mathcal{D}U e^{-S(T)} \prod_f \mathrm{Det} M(m_f, T, \mu_f),$$
(1)

where m_f is the mass of quark flavor f. $S(T)$ denotes the gluon part of the action and M is the (lattice discretized) Dirac operator. The expectation value of an operator J is

---

*Electronic address: sgupta@theory.tifr.res.in
†Electronic address: rajarshi@theory.tifr.res.in

defined as

$$\langle J \rangle \equiv J(\{m_f\}, T, \{\mu_f\})$$
$$= \frac{1}{Z} \int \mathcal{D}U \, J e^{-S(T)} \prod_f \mathrm{Det} M(m_f, T, \mu_f), \quad (2)$$

where J may or may not contain explicit dependence on the parameters. Direct simulations are possible only along certain subspaces of the full parameter space, such as $\mathrm{Re}\mu_f = 0$ or $\mu_u = -\mu_d$. However, Taylor expansions around $\mu_f = 0$ have proven to be a good method of studying the physics for general μ_f. In the remainder of this paper we shall work mainly with the two flavor case $f \in \{u, d\}$ and with degenerate quark masses $m_u = m_d = m$. We shall go freely from the parameter space expressed in terms of μ_u and μ_d to the isoscalar chemical potential $\mu_0 = (\mu_u + \mu_d)/2$ and the isovector $\mu_3 = (\mu_u - \mu_d)/2$. These are simply related to the baryon and electric charge chemical potentials. Since we perform Taylor expansions around the point $\mu_f = 0$, all angular brackets in the rest of this paper shall mean expectation values at vanishing chemical potential. These are computable by the standard methods of lattice gauge theory.

We recall a few points about the expansion of the partition function [4,5]. The μ_f appear only in the Fermion determinant. If a matrix $M(x)$ depends on a parameter x, then the identity $\mathrm{Det}M(x) = \exp[\mathrm{tr}\ln M(x)]$ yields, $[\mathrm{Det}M(x)]' = \mathrm{Det}M(x)\mathrm{tr}M^{-1}M'$, where primes denote the derivative with respect to the parameter x. Furthermore, the identity $M^{-1}M = 1$ yields $[M^{-1}]' = -M^{-1}M'M^{-1}$. This is enough to determine the Taylor coefficients of the partition function. The first order coefficients are proportional to the quark number densities

$$\frac{\partial Z}{\partial \mu_f}\bigg|_{\mu_f=0} \equiv Z Z_1, \qquad \text{where}$$
$$Z_1 = \langle \mathcal{O}_1 \rangle = \langle \mathrm{tr} M_f^{-1} M_f' \rangle, \quad (3)$$

which is flavor independent since $m_u = m_d$. When we need to keep track of the flavor we shall use the notation $\mathcal{O}_1^{(f)}$ and obvious generalizations for higher derivatives. The second order coefficients are

$$\frac{\partial^2 Z}{\partial \mu_f \partial \mu_g}\bigg|_{\mu_f=0} = Z Z_2^{(fg)} = Z\langle \mathcal{O}_{11} + \mathcal{O}_2 \delta_{fg} \rangle \qquad \text{where}$$
$$\langle \mathcal{O}_2 \rangle = -\langle \mathrm{tr} M_f^{-1} M_f' M_f^{-1} M_f' - \mathrm{tr} M_f^{-1} M_f'' \rangle. \quad (4)$$

The notation used above is $\mathcal{O}_{11} = \mathcal{O}_1 \mathcal{O}_1$. Flavor symmetry gives two independent components—$Z_2^{uu} = Z_2^{dd} = \langle \mathcal{O}_2 + \mathcal{O}_{11} \rangle$ and $Z_2^{ud} = \langle \mathcal{O}_{11} \rangle$. Expansions for isoscalar ($\mu_u = \mu_d = \mu_0$) and isovector ($\mu_u = -\mu_d = \mu_3$) chemical potentials are

$$Z(m, T, \mu_u, \mu_d)$$
$$= Z(m, T, 0, 0)\begin{cases} 1 + \langle 2\mathcal{O}_{11} + \mathcal{O}_2 \rangle \mu_0^2 + \mathcal{O}(\mu_0^4), \\ 1 + \langle \mathcal{O}_2 \rangle \mu_3^2 + \mathcal{O}(\mu_3^4). \end{cases} \quad (5)$$

The terms of odd order vanish by CP symmetry. Diagrammatic representations of these operators have been written down [13] and can be extended to other operators, as we outline later.

The double series expansion in terms of μ_u and μ_d of the pressure, $P = T(\log Z)/V$, has as coefficients the quark number densities, $n_f = (T/V)\langle \mathcal{O}_1 \rangle = 0$, and the quark number susceptibilities. The two independent linear susceptibilities [6] are the diagonal ones $\chi_{uu} = \chi_{dd} = (T/V)\langle \mathcal{O}_{11} + \mathcal{O}_2 \rangle$ arising from taking two derivatives with respect to the same chemical potential, and the off-diagonal $\chi_{ud} = (T/V)\langle \mathcal{O}_{11} \rangle$. In writing these expressions we have used the fact that the expansion is around $\mu_f = 0$. Higher order susceptibilities have also been used [4].

Similar Taylor expansions can be written for any operator J. Here we write this out to second order. Using the notation $J^{(f)}$ for the first derivative of J with respect to any explicit appearance of μ_f in it, and $J^{(fg)}$ for the explicit double derivative with respect to μ_f and μ_g we can write the first two Taylor coefficients in the expansion

$$J_1^{(f)} \equiv \frac{\partial J}{\partial \mu_f}\bigg|_{\mu_f=0} = \langle \mathcal{O}_1^{(f)} J + J^{(f)} \rangle,$$
$$J_2^{(fg)} \equiv \frac{\partial^2 J}{\partial \mu_f \partial \mu_g}\bigg|_{\mu_f=0} = \langle (\mathcal{O}_{11} + \delta_{fg}\mathcal{O}_2) J \quad (6)$$
$$+ \mathcal{O}_1(J^{(f)} + J^{(g)}) + J^{(fg)} \rangle.$$

The corresponding Taylor expansion is

$$J(m, T, \mu_u, \mu_d) = J_0 + J_1^{(u)}\mu_u + J_1^{(d)}\mu_d$$
$$+ \frac{1}{2}[(J_2^{(uu)} - J_0 Z_2^{(uu)})\mu_u^2$$
$$+ (J_2^{(dd)} - J_0 Z_2^{(dd)})\mu_d^2$$
$$+ 2(J_2^{(ud)} - J_0 Z_2^{(ud)})\mu_u\mu_d] + \cdots \quad (7)$$

where $J_0 = J(m, T, 0, 0)$. CP symmetry cannot be used to simplify the expansion in general, since the operator may not transform nicely under CP. Special simplifications occur for purely gluon operators, as we discuss later.

A. Pure gauge operators

Since pure gauge operators have no explicit dependence on the chemical potentials,

$$J_1 = \langle \mathcal{O}_1 J \rangle \quad \text{and} \quad J_2^{(fg)} = \langle (\mathcal{O}_{11} + \delta_{fg}\mathcal{O}_2) J \rangle. \quad (8)$$

The corresponding Taylor expansion is

$$J(m, T, \mu_u, \mu_d) = J_0 + J_1(\mu_u + \mu_d)$$
$$+ \frac{1}{2}[(J_2^{(uu)} - J_0 Z_2^{(uu)})(\mu_u^2 + \mu_d^2)$$
$$+ 2(J_2^{(ud)} - J_0 Z_2^{(ud)})\mu_u \mu_d] + \cdots \quad (9)$$

In general the linear term vanishes exactly only when $\mu_0 = 0$. However, for CP even operators, such as real parts of traces of products of links, the odd order terms can be shown to vanish by summing over CP orbits before performing the remaining part of the path integral.

B. Chiral Condensate

From the flavored condensates $\langle \overline{u}u \rangle$ and $\langle \overline{d}d \rangle$, one can build the isoscalar and isovector condensates which are, respectively,

$$C_S(m, T, \mu_u, \mu_d) = \frac{1}{2}[\langle \overline{u}u \rangle + \langle \overline{d}d \rangle] \quad \text{and}$$
$$\quad (10)$$
$$C_V(m, T, \mu_u, \mu_d) = \frac{1}{2}[\langle \overline{u}u \rangle - \langle \overline{d}d \rangle].$$

For equal mass quarks, C_V vanishes at vanishing chemical potential. This vector flavor symmetry is not broken by μ_0 since a sign flip in μ_0 carries the quark of each flavor to its own antiquark. As a result, C_V vanishes at all μ_0, and the series expansion for $C_S(\mu_0)$ is even. A sign flip in μ_3 carries a quark of a given flavor to the antiquark of the opposite flavor, thus mixing the vector flavor symmetry with CP. The same arguments can still be followed through to show that C_V vanishes to all orders in the expansion around $\mu_3 = 0$ and $C_S(\mu_3)$ is even. In the remainder of this paper we consider only C_S.

Recall that the quark condensate can also be written as

$$C_S(m, T, \mu_u, \mu_f) = \frac{1}{2V_4}\left(\frac{\partial \log Z}{\partial m_u} + \frac{\partial \log Z}{\partial m_d}\right)\bigg|_{m_u=m_d=m} \quad (11)$$

where V_4 is the 4-volume of the lattice [14]. Spontaneous breaking of chiral symmetry is signaled by a nonzero value of the condensate in the limit $m = 0$. We shall not be concerned with this limit in this paper, and can consequently neglect the known subtleties of taking the limits $m \to 0$ and $V_4 \to \infty$. We shall, however, check that in actual numerical work the volumes are large enough to obtain correct physical results.

Since the mass is subject to renormalization as the cutoff changes, one must bother about cutoff dependence of the condensate as well as its Taylor coefficients. Since we work with staggered quarks, the mass renormalization is multiplicative, $m_R(a) = \sqrt{Z_m}(a)m$, where the renormalization constant depends on the ultraviolet cutoff, the lattice spacing a, but not on T and μ. Throughout this paper we write the bare quark mass as m. The quark condensate is also renormalized by Z_m. If we are not interested in the absolute value of the condensate, but

only on its variation with μ at constant T, then one can simply work with either of the ratios

$$\frac{C_S(m_R, T, \mu_u, \mu_d; a)}{C_S(m_R, 0, 0, 0; a)} \quad \text{(Z scheme)} \quad \text{or}$$

$$\frac{C_S(m_R, T, \mu_u, \mu_d; a)}{C_S(m_R, T, 0, 0; a)} \quad \text{(T scheme).} \quad (12)$$

One expects the T scheme to be undefined for $T > T_c$ when $m_R = 0$, since the chiral condensate then vanishes. Elsewhere there is a finite multiplicative relation between the schemes which has the interpretation of the T-dependence of C_S at $\mu = 0$. The computations have to be performed at fixed renormalized mass. We perform a formal expansion here which will later be renormalized in either of these schemes.

For the u quark condensate $\langle C_u \rangle = \langle \overline{u}u \rangle = \langle \mathrm{Retr}M_u^{-1} \rangle$, clearly $C_u^{(d)} = C_u^{(ud)} = C_u^{(dd)} = 0$. The nonvanishing derivatives are $C_u^{(u)} = -\mathrm{Retr}M_u^{-1}M_u'M_u^{-1} = C'$ and $C_u^{(uu)} = \mathrm{Retr}(2M_u^{-1}M_u'M_u^{-1}M_u'M_u^{-1} - M_u^{-1}M_u''M_u^{-1}) = C''$. For the d quark condensate, the corresponding relations can be found by flipping u and d indices. Since the Taylor series expansion is carried out at $\mu = 0$, in the limit of degenerate masses the quantities C' and C'' are flavor independent. In this limit the Taylor expansion coefficients of the flavored condensates are flavor independent, and we need to evaluate the four quantities

$$C_S^0 = \langle C \rangle,$$
$$C_S^1 = \langle 2\mathcal{O}_1 C + C' \rangle,$$
$$C_S^{20} = \langle 2(\mathcal{O}_{11} + \mathcal{O}_2)C + 2\mathcal{O}_1 C' + C'' \rangle$$
$$\quad - 2\langle \mathcal{O}_{11} + \mathcal{O}_2 \rangle\langle C \rangle,$$
$$C_S^{11} = 2\langle \mathcal{O}_{11} C + \mathcal{O}_1 C' \rangle - 2\langle \mathcal{O}_{11} \rangle\langle C \rangle,$$
$$\quad (13)$$

A direct check shows that C_S^1 vanishes, as does every odd term in the expansion. C_S^{20} is the diagonal, and C_S^{11} is the off-diagonal QRC.

A diagrammatic representation of the expansion of the chiral condensate is shown in Fig. 1. This builds on a previous diagrammatic representation of the expansion of the partition function [13]. Every line denotes a fermion propagator, a dot denotes a derivative with respect to μ_f (an insertion of γ_0 in the continuum), every cross is a derivative with respect to m_f (a mass insertion), and every closed line is a trace over Fermion coordinates. The fermions have to be dressed in all possible ways by gluon insertions. Power counting arguments [15] can be easily extended to estimate the power of the gauge coupling g associated with the connected parts which appear in Eq. (13) when they are evaluated at high temperatures. The largest quark-loop-disconnected quantity is $\langle \mathcal{O}_2 C \rangle_c$ which is of order g^4. Both $\langle \mathcal{O}_{11} \rangle$ and $\langle \mathcal{O}_1 C' \rangle_c$ are of order g^6, and $\langle \mathcal{O}_{11} C \rangle_c$ is of order g^8. These powers may be modified by $\log g$ terms due to infrared singularities. $\langle C'' \rangle$ is of order g^0, and, because it is nonvanishing,
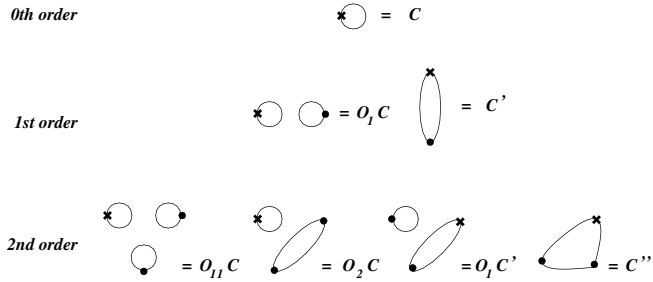
FIG. 1. A diagrammatic representation of the terms in the expansion of the chiral condensate, extending the rules in [13]. The lines represent quark propagators. The dots are insertions of M' (which is γ_0 in the continuum limit) and the crosses are mass insertions. They represent derivatives with respect to μ and m respectively. The contribution of each topology to the derivatives in Eq. (13) can be found by simple counting. Every closed loop is a Fermion trace. These diagrams should be thought of as being connected to all possible topologies of gluons.

generically gives the largest contribution in the high temperature phase.

The Taylor expansions of C_S are

$$C_S(m, T, \mu_0) = C_S^0 + (C_S^{20} + C_S^{11})\frac{\mu_0^2}{2} + \cdots,$$

$$C_S(m, T, \mu_3) = C_S^0 + (C_S^{20} - C_S^{11})\frac{\mu_3^2}{2} + \cdots \quad (14)$$

where the temperature dependence of the coefficients has not been shown explicitly. Note that in the T scheme the Taylor series begin with a constant term of exactly unity. In this scheme one can rewrite the series as an expansion in μ/T and render all the coefficients dimensionless. Then the remaining Taylor coefficients have the significance of fractional changes due to nonzero values of μ. The power counting argument shows that for $T \gg T_c$ the coefficient of the quadratic term is dominated by the operators $\langle C'' \rangle_c$, and the two expansions differ only by terms subleading in g. In the low-temperature phase these arguments fail, and the two series could have significantly different behavior. Near and below T_c other arguments, outlined in Sec. IV, also lead us to expect different behavior for the two series.

C. Chiral Ward identities for meson susceptibilities

A meson operator is $M(\mathbf{x}) = \overline{\psi}(\mathbf{x})\Gamma\psi(\mathbf{x})$, where ψ is a quark field operator and Γ is a Hermitian spin-flavor matrix. The conjugate operator is $M^\dagger(\mathbf{x}) = \psi^\dagger\Gamma^\dagger\gamma_0\psi = \overline{\psi}\tilde{\Gamma}\psi = \pm\overline{\psi}\Gamma\psi$, where the plus sign is obtained for the Dirac matrices 1, γ_0, and $\gamma_5\gamma_0$ and the negative sign for γ_5, γ_i, and $\gamma_5\gamma_i$. The meson correlators are

$$C(\mathbf{x}, \mathbf{y}) = \langle M(\mathbf{x})M^\dagger(\mathbf{y})\rangle = \langle \text{tr}\Gamma M^{-1}\Pi(\mathbf{y})\tilde{\Gamma}(M^\dagger)^{-1}\Pi(\mathbf{x})\rangle, \quad (15)$$

where M is the Dirac operator, and $\Pi(\mathbf{x})$ is the projector to one site $\mathbf{x}$. The final expression on the right was obtained using the relation $\Pi^2 = \Pi$ and the fact that Π and Γ commute since they act on different spaces. In [7] the correlator was parametrized in the form $A\cosh m(L/2 - x)$ and the derivatives with respect to μ of the parameters A and m were related to operator expectation values obtained by taking derivatives of the right-hand side of Eq. (15). However, since CP symmetry is explicitly broken on introduction of chemical potentials, one need no longer have $C(\mathbf{x}, \mathbf{y}) = C(|\mathbf{x} - \mathbf{y}|)$. This is explicitly visible in the computations reported in [16,17].

A little tinkering does not help, since it is the transfer matrix formalism that needs to be reexamined at finite μ, because a nonzero value of this parameter introduces an explicit breaking of time reversal symmetry. It is much more straightforward to deal with the meson susceptibilities [18],

$$\chi_\Gamma = \frac{1}{V}\sum_{\mathbf{xy}} C(\mathbf{x}, \mathbf{y}) = \frac{1}{V}\langle \text{tr}\Gamma M^{-1}\tilde{\Gamma}(M^\dagger)^{-1}\rangle. \quad (16)$$

If a single pole dominates this propagator then the corresponding mass, $m_\Gamma \propto 1/\sqrt{\chi_\Gamma}$. However, this quantity more generally measures mesonic fluctuations [18].

Chiral Ward identities are consequences of certain operator equalities which follow from chiral symmetries. Each formulation of lattice fermions can preserve a different subset of these identities; a basic set for staggered fermions can be found in [19]. The remaining continuum identities are violated at finite lattice spacing, and hence can be used to check the approach to the continuum. The prototypical chiral Ward identity is $C_S(T, \mu) = m\chi_\pi(T, \mu)$, where χ_π is the pseudoscalar susceptibility. Furthermore, this chiral Ward identity allows us to define a renormalized χ_π using the simultaneous renormalization of the quark mass and the condensate. Taylor expansions of both sides of this identity can then be equated term by term. Another conclusion is that the Taylor expansion of χ_π must be even in μ. Explicit construction of the first Taylor coefficient shows that it vanishes, in conformity with this proof.

A second chiral Ward identity [20] relates the isovector scalar susceptibility to the mass derivative of the condensate: $\partial C_S/\partial m = -\chi_\epsilon$. Again this can be used to renormalize χ_ϵ and relate two Taylor series. We emphasize that this involves the isovector scalar, i.e., the scalar meson susceptibility implicated here is obtained out of a connected quark loop.

We show later that in the continuum limit of the high temperature phase the second derivatives of the condensate with respect to the chemical potential vanish. As a result, the QNS are insensitive to variations of the quark mass, and the pion susceptibilities are insensitive to chemical potential. Also, in this phase, symmetry argu-

ments show that $\chi_\pi = \chi_\epsilon$ [21], implying that C_S vanishes linearly with m. As a result, we can deduce that the scalar susceptibility is also independent of the isoscalar chemical potential, at least to quadratic order. Below T_c this chain of logic does not hold. The scalar susceptibility is interesting because of speculation about the massless modes at the critical end point [22]. We will discuss it at greater length elsewhere.

D. Maxwell relations

A Maxwell relation is the equality of two distinct physical interpretations of a mixed derivative obtained by interchanging the order of the derivatives. From the Taylor expansion of the chiral condensate in Eq. (14) we can find Maxwell relations with the change of quark number susceptibilities with the quark mass. The leading order relation

$$\frac{\partial \langle \overline{\psi}\psi \rangle_S}{\partial \mu} = \frac{\partial n}{\partial m} \qquad (17)$$

was first noted in [23]. It is trivially true at $\mu = 0$ since the first derivative on the left vanishes, as does n for all quark masses.

The second derivatives give two nontrivial Maxwell relations and consequent relations using the chiral Ward identities discussed earlier,

$$
\begin{aligned}
C_S^{20} &= \frac{\partial^2 \langle \overline{\psi}\psi \rangle_S}{\partial \mu_u^2} = m \frac{\partial^2 \chi_\pi}{\partial \mu_u^2} = \frac{\partial \chi_{uu}}{\partial m}, \\
C_S^{11} &= \frac{\partial^2 \langle \overline{\psi}\psi \rangle_S}{\partial \mu_u \partial \mu_d} = m \frac{\partial^2 \chi_\pi}{\partial \mu_u \partial \mu_d} = \frac{\partial \chi_{ud}}{\partial m}.
\end{aligned}
\qquad (18)
$$

There are higher order relations between the mass derivative of the nonlinear susceptibilities and the higher Taylor coefficients of the condensate. This class of Maxwell relations can be checked by explicit differentiation.

Preliminary results have been reported in [24] and a mixed version of this has been used later to correct for the mass dependence of a Taylor expansion of the pressure [25]. Here, as a by-product of our computation of the renormalized chiral condensate, we shall give the continuum limit of the derivative of the susceptibility.

The relative rates of strange and light quark production in heavy-ion collisions [26] is

$$\lambda_s = \frac{\chi_{ss}}{\chi_{uu}}, \qquad (19)$$

with obvious extensions to the production rates of heavier quarks. Since it is hard to perform lattice computations at realistic values of light quark masses due to constraints of computer time, one can lighten the computational burden by using a Taylor series for the mass dependence of the susceptibilities utilizing the above Maxwell relation. Then one can compute λ_s at some reasonably light quark mass, corresponding to, say, the pion mass being 2 to 3 times heavier than in the real world, and extrapolate to the physical quark mass values using the Maxwell relation. One can also investigate the stability against small variations in the heavy quark mass by similar means.

III. RESULTS

A. Implementing the renormalization scheme

In Eq. (12) we have defined a renormalization scheme in which the multiplicative renormalization of the chiral condensate at temperature T and chemical potential μ is absorbed by the bare condensate at $T = 0$ or $\mu = 0$ evaluated at the same lattice spacing a. In order to implement this scheme this compensation must be performed at a constant renormalized quark mass. We complete the renormalization prescription by choosing to trade the pion mass for the renormalized quark mass. The practical

TABLE I. Meson masses in quenched QCD with Wilson action and staggered quarks. The χ^2 for pions is obtained by fitting local masses to a constant. The rho meson mass is obtained with a four parameter fit to the vector correlator. Details are discussed in the text.

aT_c	β	Size	am_q	$a^2 m_\pi^2$	χ^2	Range	am_ρ	χ^2	Range	m_π/m_ρ
0.1667	5.8941	$16^3 \times 32$	0.01667	0.119(1)	1.99	7–10	0.66(2)	1.43	5–17	0.52(2)
			0.02	0.141(2)	2.82	7–10	0.68(2)	1.72	5–17	0.55(2)
			0.03	0.205(2)	1.39	8–10	0.74(2)	2.54	5–17	0.61(2)
		30^4	0.01667	0.123(3)	4.41	6–11	0.71(4)	10.73	3–16	0.49(3)
			0.02	0.142(2)	5.59	6–10	0.72(3)	11.08	3–16	0.52(2)
			0.03	0.214(4)	4.10	6–11	0.77(3)	11.78	3–16	0.60(2)
0.1333	6.0150	$20^3 \times 40$	0.01333	0.080(1)	1.66	7–13	0.56(2)	4.95	5–21	0.50(2)
0.1111	6.14	$24^3 \times 48$	0.01111	0.0515(9)	1.64	9–13	0.42(1)	2.62	7–25	0.54(1)
0.0833	6.3384	40^4	0.0083	0.035(1)	6.58	9–17	0.333(9)	2.55	7–21	0.56(2)
			0.01	0.040(1)	5.06	10–17	0.341(8)	2.64	7–21	0.59(2)
0.0667	6.525	42^4	0.0067	0.022(1)	2.45	13–-19	0.25(1)	7.35	8–22	0.60(3)
			0.005	0.018(1)	2.85	13–19	0.25(1)	6.67	8–22	0.54(3)
0.0556	6.65	50^4	0.0056	0.0161(3)	8.13	13–23	0.21(1)	15.0	10–25	0.60(3)

question is then the choice of the bare quark mass which corresponds to a fixed pion mass.

The lattice spacing has been connected to the temperature scale using the QCD β-function at full two-loop order [27]. This scale determination was used to tune the bare couplings in the Wilson action required to simulate the quenched theory at a fixed physical temperature while changing the lattice spacing [28]. Here we used the same bare couplings to extract the pion mass using $T = 0$ simulations.

The series of bare couplings used correspond to fixed $T = 1.5T_c$ on lattices with $N_t = 4, 8, 10,$ and 12 and to fixed $T = 0.75T_c$ for $N_t = 8, 10,$ and 12. The lattice sizes L were selected so that $Lm_\pi \gtrsim 6$ in order to keep finite volume effects under control. At the two coarsest lattice spacings a previous determination of meson masses [29] could be used to estimate m_π and select an appropriate value of L. Then one could successively use the already determined masses to estimate the size which would be required at finer lattice spacing. Quenched configurations were generated using the Wilson action. At each lattice spacing the first 500–1000 sweeps were discarded for thermalization and a configuration was kept after every subsequent 50 sweeps.

The stored configurations were used to determine the chiral condensate, through a noisy evaluation of the trace of the inverse of the fermion matrix, and meson correlators. The stopping criterion on the staggered fermion matrix inversion was decreased by factors of ten until the extracted value of m_π was seen to stabilize. It was observed that while decreasing lattice spacing keeping m_π fixed, the stopping criterion had to be decreased significantly. We attribute this to the fact that as the lattice spacing decreases at zero temperature the eigenvalues near a rapidly decreasing renormalized quark mass take more conjugate gradient steps to resolve.

Our extraction of pion masses was based on effective (local) mass extraction $m(t)$, and cross checked by fits. As has been known for a long time, this is contaminated at small distances by higher lying states and at large distances by periodic lattice artifacts. When a plateau can be seen, that value is taken as an estimate of the ground state mass. We converted this into an automatic task by varying t_{min} and t_{max} and for each fixed value of this parameter checking whether the data on $m(t)$ could be fitted to a constant. We accepted the largest interval over which this could be done and took the corresponding constant as an estimate of the mass (see Table I). For the vector meson the local mass is harder to stabilize, and we used four parameter fits to extract the mass, varying the fit interval to look for stability.

In simulations at the coarser lattice spacings we performed a series of computations at larger bare quark mass. These are useful in order to check that the lattice volumes are under control. The near constancy of the ratio

$a^2m_\pi^2/(am_q)$ at fixed a on the coarser lattices indicates that the lattice volumes are sufficiently large that one can extrapolate to the correct continuum physics.

In simulations at a sequence of lattice spacings a corresponding to a fixed temperature and varying N_t ($a = 1/TN_t$), with a sequence of bare quark masses $m/T_c = 0.1$, we found that the dimensionless ratio m_π^2/mT is fixed. This is shown in Fig. 2. The constancy of this ratio shows that this sequence of bare quark masses corresponds to a fixed renormalized quark mass, and gives an easy method to tune the bare quark mass in order to fix the renormalized quark mass. At this quark mass, we found that $m_\pi/m_\rho \approx 0.6$, indicating that m_ρ could also have been chosen to fix the renormalized quark mass. For the parameters chosen here, the fact that the renormalized quark mass is rather heavy is seen both in the fact that the ratio m_π/m_ρ is larger than the physical value and also in that $m_\pi/T_c \approx 2.3$. We recall that with two flavors of dynamical staggered quarks choosing $m/T_c = 0.1$ corresponds to $m_\pi/m_\rho = 0.36 \pm 0.01$, and that on reducing the bare quark mass to $m/T_c = 0.03$ the ratio m_π/T_c became physical [30].

B. Continuum limit in quenched QCD

1. T > T_c

We used stored gauge configurations from the study in [28] for our measurements. These were obtained on $N_t = 4, 8, 10, 12,$ and 14 lattices for temperatures $T = 1.5T_c, 2T_c,$ and $3T_c$ respectively. The main concern in choosing the spatial size N_s is to avoid gross distortions of the infinite volume result. For this it is sufficient to have $N_s/N_t > \max(2, T/T_c)$. For $N_t = 4$ we have used $N_s = 12$. For all the other N_t the spatial size was chosen to be
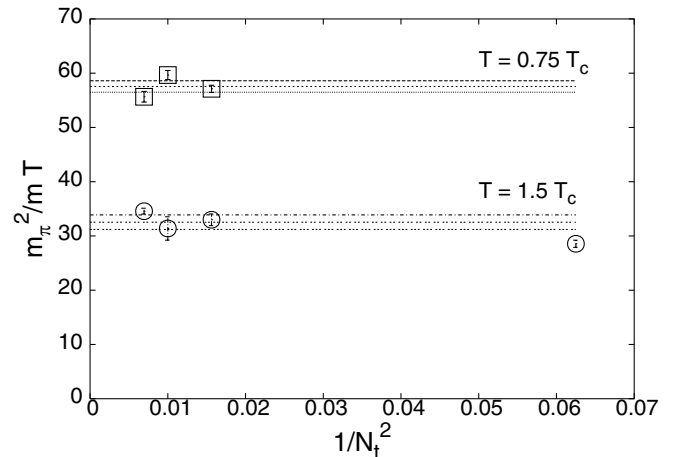

FIG. 2. The dimensionless ratio $m_\pi^2(T = 0)/mT$ for fixed bare quark mass $m/T_c = 0.1$ at a succession of lattice spacings corresponding to fixed $T = 1.5T_c$ at varying N_t shown as a function of $1/N_t^2 = a^2T^2$. The constancy of the ratio shows that this procedure correctly holds the renormalized quark mass constant and thereby implements the renormalization scheme of Eq. (12).

$N_s = 2N_t + 2$ for $T/T_c = 1.5$ and 2, and $N_s = 3N_t + 2$ for $T/T_c = 3$. For details of the generation of the configurations and their statistical properties, we refer the reader to [28]. In this work we recomputed, as a check, the operators $\mathcal{O}_1$, $\mathcal{O}_{11}$, and $\mathcal{O}_2$ which were studied in [28] and supplemented these by computations of C, C', and C'' needed for the computation of the Taylor expansion of the chiral condensate. The traces were evaluated by the noisy method (see [28] for details). For the conjugate gradient algorithm to obtain the matrix inverses, we used a stopping criterion that the norm of the residual should be less than $10^{-3}\sqrt{N_t N_s^3}$.

The vanishing of the expectation values $\langle\mathcal{O}_1\rangle$ and $\langle C'\rangle$ are checks of the accuracy of the computation. On each lattice and at every temperature, we found that the expectation values were zero to within a part in 10^6 with the above stopping criterion. In the high temperature phase of QCD, where we work, χ_{ud} is small, and therefore one expects a noisy and almost vanishing signal for its derivative with respect to the quark mass. In agreement with this expectation, we find that C_S^{11} is too small and noisy to be measured. We return to this in Sec. IV.

The diagonal QRC in the T scheme is shown in Fig. 3. It is clear that there is significant μ-dependence on coarser lattices; in fact for $N_t = 4$ we found that $T^2 C_S^{20}(T)/C_S(T) \simeq -0.096$ at $T/T_c = 1.5$. However, this Taylor coefficient vanishes at the 99% confidence limit on extrapolation to the continuum. The conversion from T scheme to Z scheme involves a finite multiplicative factor $C_S(m_R, T)/C_S(m_R, 0)$ which also has an interpretation as the temperature dependence of the condensate. At $T = 1.5T_c$ we find on extrapolation to the continuum that this factor is 0.26 ± 0.01 for m_R such that $m_\pi/m_\rho \approx 0.6$. With decreasing quark mass this factor is expected to decrease.

A vanishing continuum limit of the QRC is also found for $m/T_c = 0.1$ at the two other temperatures that we have studied. The identities in Eq. (18) then imply that χ_{uu} is insensitive to changes in the quark mass and χ_π is insensitive to μ in this range of temperatures. Since χ_{uu} agrees with a perturbative evaluation for $T \gtrsim 1.5T_c$, its insensitivity to m can be understood from the fact that the effective infrared cutoff is given by the Matsubara frequency πT and not by m when $m/T_c < \pi T/T_c$.

2. T < T_c

We also made a series of simulations at fixed $T/T_c = 0.75$ for $N_t = 6$, 8, 10, and 12 in quenched QCD with the Wilson action. Three hits of pseudo-heat-bath followed by one Metropolis step made up one composite sweep. The first 500 sweeps were discarded for thermalization and subsequently one configuration was saved once every 500 sweeps. Between 35 and 45 such stored configurations were used on each lattice for this work. Measurements were made with the bare quark mass $m/T_c = 0.1$ and with 50 noise vectors for evaluation of quark traces. In all cases we used spatial sizes $N_s = 2N_t$. From the $T = 0$ runs described earlier, it can be seen that the size of the spatial box corresponds to over 5.5 pion Compton wavelengths (at $T = 0$) and hence finite size effects are under reasonable control.

We found that the continuum limit of both $\langle\mathcal{O}_2\rangle$ and $\langle\mathcal{O}_{11}\rangle$ were consistent with zero within reasonably small errors. On all but the coarsest lattice, $N_t = 6$, the first expectation value was significantly smaller than the second. As a consequence χ_{ud} and χ_{uu} were equal within errors even at finite lattice spacing. As shown in Fig. 4, C_S^{20} also vanishes within errors in the continuum limit, showing that the vanishing of χ_{uu} is not an accident of the
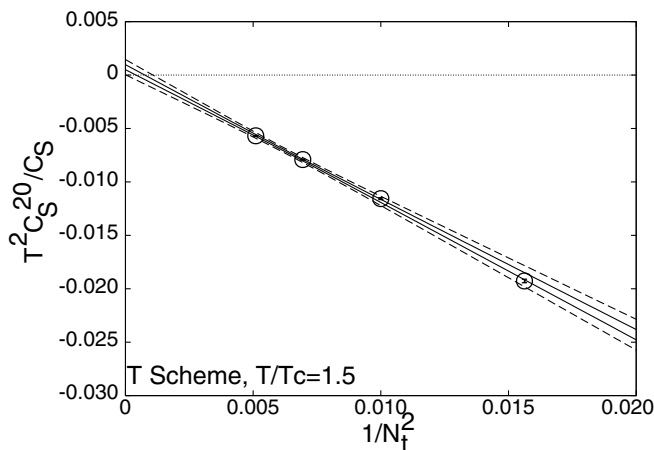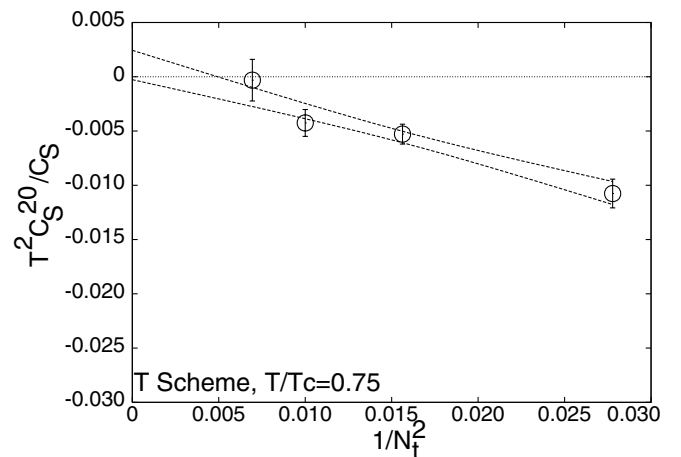

FIG. 3. The diagonal QRC in the T scheme at fixed $T/T_c = 1.5$ holding the renormalized quark mass fixed by fixing the bare mass to be $m/T_c = 0.1$. The full lines show the 1-σ band on the continuum extrapolation and the dashed lines show the 3-σ confidence band.

FIG. 4. The diagonal QRC in the T scheme at fixed $T/T_c = 0.75$ holding the renormalized quark mass fixed by fixing the bare mass to be $m/T_c = 0.1$. The lines show the 1-σ band on the continuum extrapolation.

choice of the quark mass. The off-diagonal QRC was consistent with zero at each N_t.

C. Dynamical staggered quarks

We report the results of a series of computations with two flavors of dynamical quarks as the temperature varies between $0.75T_c$ and $2T_c$. The simulations were performed using the R-algorithm with two flavors of quarks with bare mass of $0.1T_c$, corresponding to $m_\pi/m_\rho = 0.36 \pm 0.01$ [30]. Three lattice sizes were used in most of the simulations, namely 4×8^3, 4×12^3, and 4×16^3. The critical coupling β_c for $N_t = 4$ was determined in [31] and the setting of the temperature scale was performed by methods given in [30]. The critical coupling for this quark mass was seen in the peaks of χ_ϵ, the Wilson line susceptibility, and even in autocorrelation times [30,31]. The critical coupling is also consistent with those found for neighboring values of quark mass in [30–32].

Lattice computations with dynamical quarks are still too costly for the continuum limit to be taken easily. However, in order to have some idea of the continuum limit we have also performed two further simulations with 6×12^3 and 8×16^3 lattices at $T = 0.9T_c$. In addition, we have results at T_c on 6×12^3 lattices. The critical couplings at these N_t were determined in [33]. It is impossible to collect a sufficient number of statistically independent configurations on $N_t = 8$ lattices near T_c with current computing resources due to a rapid increase in autocorrelation times, τ. In all our simulations autocorrelations of local observables were monitored and the total run length was at least 50 times the longest, τ_{max}, when measured self consistently over the history. The measurements used between 50 and 250 configurations, each separated by τ_{max}. We work in the Z scheme since we are interested in the T dependence of the derivatives.

Consistent with our previous observations, C_S^1 was seen to vanish with small errors across the full range of temperatures considered. The diagonal QRC was negative and differed significantly from zero, as shown in Fig. 5. For comparison, results from the quenched theory at the same bare quark mass are also shown. The T-dependence is seen to be a little different; this could reflect either the difference in the value of m_π/m_ρ or be a quenching artifact. The off-diagonal QRC (see Fig. 6) is consistent with zero within small errors above T_c. Near and below T_c larger fluctuations are seen. Although still consistent with zero at the 3-σ level, the averages increase by several orders of magnitude compared to $T > T_c$, and seem to be comparable in magnitude to the diagonal QRC.

The results of our preliminary investigation of the continuum limit with dynamical quarks are shown in Fig. 7. At $0.9T_c$ the 3-σ error band on the extrapolation of the diagonal QRC is consistent with zero. At T_c the continuum extrapolation perforce had to be performed with data from only two lattice spacings. These com-
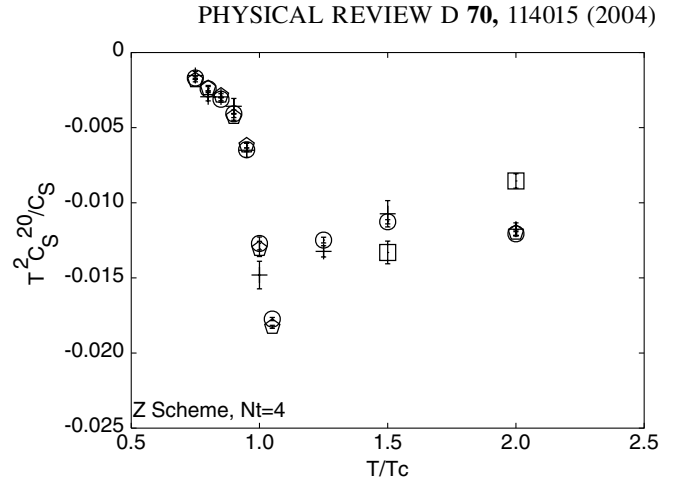

FIG. 5. The diagonal QRC as a function of the temperature in $N_f = 2$ QCD within the Z scheme, for $a = 1/4T$ holding the renormalized quark mass fixed by fixing the bare mass to be $m/T_c = 0.1$. Pluses denote results obtained on 4×8^3 lattices, pentagons on 4×12^3 and circles on 4×16^3. The boxes represent the quenched QCD value.

pletely fix the parameters of a linear extrapolation to the continuum. Error estimates were obtained by then taking the slope as this given parameter and estimating the error on the continuum value in the usual way. The resulting 1-σ and 3-σ error limits on the extrapolation are shown in Fig. 7. Another estimate is to take the extrapolations of the upper end of one error bar and the lower end of the other. This lies within the 3-σ band given. With all these caveats, our data currently points to a nonzero continuum extrapolation of renormalized C_S^{20} at T_c.
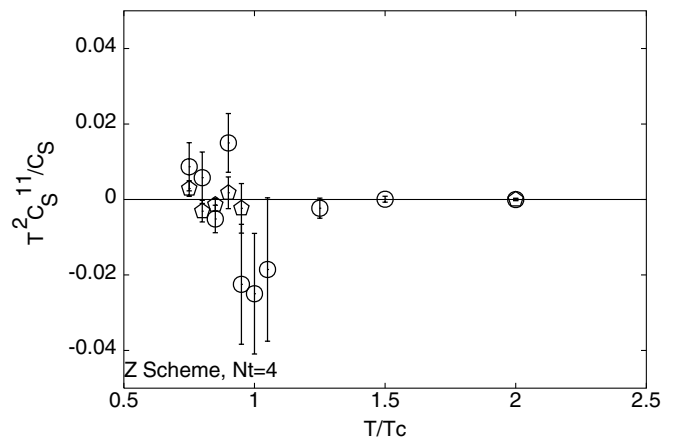

FIG. 6. The off-diagonal QRC as a function of the temperature in $N_f = 2$ QCD within the Z scheme, for $a = 1/4T$ holding the renormalized quark mass fixed by fixing the bare mass to be $m/T_c = 0.1$. Pentagons represent results for 4×12^3, and circles for 4×16^3.
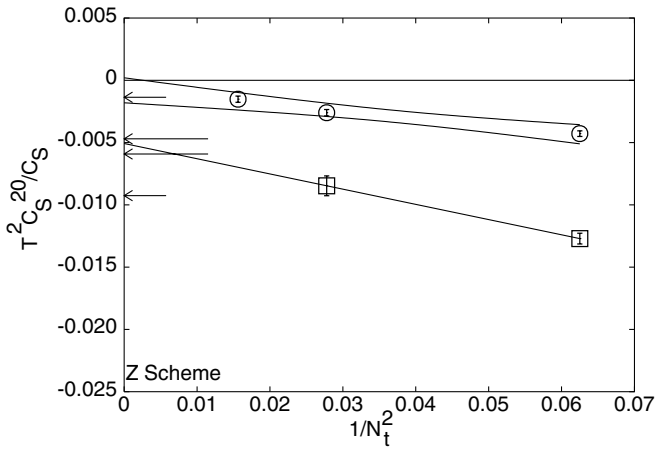
FIG. 7. The continuum extrapolation of the diagonal QRC renormalized in the Z scheme in $N_f = 2$ QCD with bare quark mass of $0.1T_c$. The circles denote data for $T = 0.9T_c$, and the 3-σ band for the continuum extrapolation is shown. The boxes represent data at T_c, and the 1-σ (nearer arrows) and 3-σ (further arrows) limits of the extrapolation shown are discussed in the text.

IV. DISCUSSION

The chiral condensate is a derivative of the free energy density with respect to quark mass [Eq. (11)], and the latter requires renormalization. As a result, so does the condensate and its Taylor coefficients. We have defined two renormalization schemes for staggered quarks [Eq. (12)] in order to set up a well defined Taylor series expansion for the chiral condensate as a function of the chemical potential μ [Eqs. (13) and (14)]. Diagrammatic rules for writing down the operators defining the Taylor coefficients have been given (Fig. 1). The first order Taylor coefficient C_S^1 vanishes by symmetry. The two QRCs are related through Maxwell relations and chiral Ward identities to all other second order Taylor coefficients in the chiral sector [Eq. (18)]. The diagonal QRC C_S^{20} has small errors and is easily measurable at the renormalized quark mass we used. We found that at finite lattice cutoff it is negative. Away from T_c, both in quenched and $N_f = 2$ QCD, the continuum limit of this quantity vanishes. We have presented evidence (Fig. 7) that near T_c in the $N_f = 2$ theory it does not vanish.

This negative peak in C_S^{20} (Figs. 5 and 7) corresponds to a significant shift of the condensate, and hence χ_π, with chemical potential. The implications for strangeness production have been pointed out in Sec. II D. Here we discuss how measurements of the diagonal and off-diagonal QRCs, C_S^{20} and C_S^{11}, test current conjectures about the phase diagram of QCD at small μ based on the perturbative expansion or model computations [8–11].

The location of T_c is often identified through a peak in the scalar susceptibility χ_ϵ (which is the same as the mass derivative of the chiral condensate through the Patel Ward

identity [20]). In the chiral limit this is a unique definition, since the direction of spontaneous symmetry breaking at low T makes this a massive particle, which becomes massless precisely at T_c. However, at finite quark mass the symmetry is explicitly broken, χ_π is finite throughout the low T phase and there is a crossover instead of a critical point along the T axis at T_c [34], as shown in the top panel of Fig. 8 (see however, [35]). The crossover temperature T_c is usually not uniquely defined, in the following sense. At a phase transition different physical quantities give exactly the same estimate of T_c. This is no longer true at a crossover. Thus the slight shift in the peak of C_S^{20} (Fig. 5) compared to T_c previously defined from peaks in χ_ϵ and the Wilson line susceptibilities [30,31] lends some support to the scenario of a crossover.

Furthermore, the observed negative peak in the quadratic response of the condensate shows that χ_π decreases at finite μ, and hence pions cannot be the soft mode as one approaches the critical end point. To the best of our knowledge, this is the first such indication from lattice QCD. Unless C_S^{20} changes sign in the continuum, this argument continues to hold. We have presented evidence that it does, because the diagonal QRC does not turn positive in the vicinity of T_c (Fig. 7). Thus support for the standard picture of the phase diagram for $m_R > 0$ is provided by
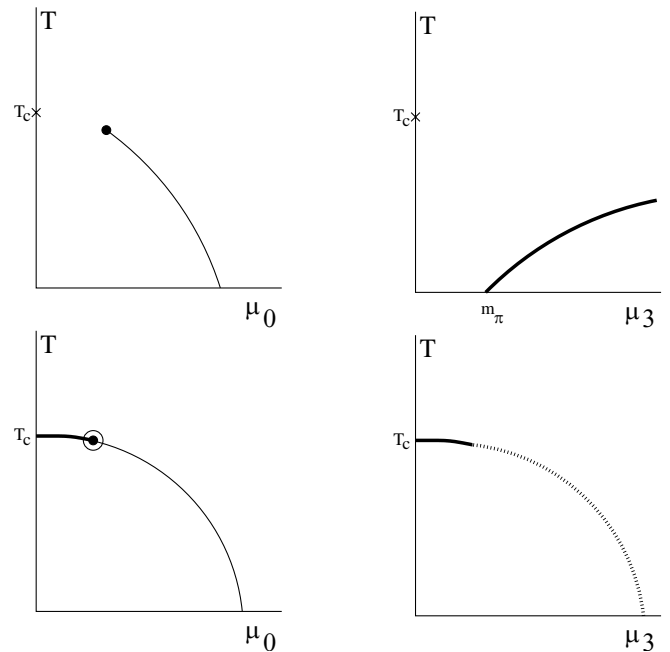

FIG. 8. The panels on top show the expected phase diagrams in the $T - \mu_0$ [8] and $T - \mu_3$ [9] planes for $m_R > 0$. The panels below show the expectations in the chiral limit, $m_R = 0$ [10,11]. Thick lines denote second order transitions, the tricritical point is marked with a fancy circle and the dotted line shows a part of the critical line which could be a model artifact [37]. Further interesting phases at large μ are not shown.

C_S^{20} in two different ways—by indicating that at $\mu = 0$ there could be a crossover, and by showing that pion fluctuations decrease as the baryon density increases.

It is interesting to see what else the QRCs can say about the phase diagram. For $m_R > 0$, as T decreases, the Taylor series for C_S will eventually hit the critical end point in an extrapolation in μ_0 [8], and the critical line in μ_3 [9,36] (see upper panels in Fig. 8). Therefore, at lower T there must be differences in the two extrapolations. This can only happen if the off-diagonal QRC becomes significant. We have shown preliminary evidence for this in Fig. 6. This should become easier to measure with decreasing m_R since m_π, as well as the chemical potential at the critical end point, are expected to decrease.

In the chiral limit the phase diagram in the $T - \mu_0$ plane is expected [8] to contain a critical line meeting the T axis at a critical point T_c. It is also expected that this critical line ends in a tricritical point where it meets a line of first order phase transitions emerging from the μ_0 axis (see lower panels in Fig. 8). The phase diagram in the $T - \mu_3$ plane has been explored in [10,11]. A second critical line is expected to emerge from the T-axis, curving down to eventually touch the μ_3 axis [37]. Since there is a unique transition along the T-axis for $\mu_0 = \mu_3 = 0$, one expects both critical lines to start from T_c.

A Taylor expansion cannot be started at the critical point T_c, but it is possible to make such a series expansion immediately above and below, and thus track the curvature of the two critical lines. If the off-diagonal QRC vanishes, then the physics along these two lines is the same. However, one has massless pions, whereas the other does not. Also, at lower temperature, one series should give evidence of a tricritical point on extrapolation, whereas the other should not. Thus, if the phase diagrams drawn above are accurate, then they should be reflected by a nonvanishing value of the off-diagonal QRC. Further, measurements of $C_S^{20} \pm C_S^{11}$ would give information on the soft modes in these two directions.

Thus, there are several extensions of this study which would be interesting to perform in the future. First, the chiral extrapolation of C_S^{20} and C_S^{11} obtained at fixed N_t by varying m_R would indicate whether the tricritical point indeed appears at $m_R = 0$. If the standard picture does hold, then the chiral extrapolation of $C_S^{20} + C_S^{11}$ and $C_S^{20} - C_S^{11}$ at T just below T_c would give information on the soft modes along the two critical lines.

ACKNOWLEDGMENTS

[1] See, for example, M. Gyulassy and L. McLerran, nucl-th/0405013; R. Rapp, J. Phys. G **30**, S951 (2004).

[2] Z. Fodor and S. Katz, Phys. Lett. B **534**, 87 (2002).

[3] M.-P. Lombardo and M. d'Elia, Phys. Rev. D **67**, 014505 (2003); Ph. de Forcrand and O. Philipsen, Nucl. Phys. **B673**, 170 (2003).

[4] R.V. Gavai and S. Gupta, Phys. Rev. D **68**, 034506 (2003); Nucl. Phys. B, Proc. Suppl. **129**, 524 (2004).

[5] C. R. Allton, *et al.*, Phys. Rev. D **68**, 014507 (2003).

[6] S. Gottlieb *et al.*, Phys. Rev. Lett., **59**, 2247 (1987).

[7] S. Choe *et al.*, Phys. Rev. D **65**, 054501 (2002).

[8] J. Berges and K. Rajagopal, Nucl. Phys. **B538**, 215 (1999); M. A. Halasz *et al.*, Phys. Rev. D **58**, 096007 (1998).

[9] D. Son and M. Stephanov, Phys. Rev. Lett. **86**, 592 (2001).

[10] B. Klein, D. Toublan, and J. J. M. Verbaarschot, Phys. Rev. D **68**, 014009 (2003).

[11] Y. Nishida, Phys. Rev. D **69**, 094501 (2004).

[12] Preliminary results for the bare Taylor coefficients of the condensate at lattice spacing $a = 1/4T$ in QCD with two flavors of quarks were presented in S. Choe *et al.*, Nucl. Phys. B, Proc. Suppl. **106**, 462 (2002).The bare series for the condensate has been also been studied earlier in the NJL model in O. Miyamura *et al.*, Phys. Rev. D **66**, 077502 (2002).

[13] S. Gupta, Acta Phys. Pol. B **33**, 4259 (2002).

[14] In most literature on lattice QCD the sign of the condensate is chosen as in Eq. (11), and C_S is therefore positive. In translating our results to the convention with negative C_S, care must be taken to absorb the sign into the multiplicative renormalization constant, so that the renormalizations of mass and chiral condensate differ by a sign. Equation (12) shows that this sign will not appear in the expansion of the condensate, but will then appear in the chiral Ward identities and the Maxwell relations.

[15] J.-P. Blaizot (private communication).

[16] S. Gupta, hep-lat/0202005.

[17] S. Hands and D. N. Walters, Phys. Rev. D **69**, 076011 (2004); S. Hands and C. G. Strouthos, Phys. Rev. D **70**, 056006 (2004).

[18] S. Gupta, Phys. Lett. B **288**, 171 (1992).

[19] G. W. Kilcup and S. Sharpe, Nucl. Phys. **B283**, 493 (1987).

[20] A. Patel, Phys. Lett. **141B**, 244 (1984).

[21] S. Gupta, Phys. Rev. D **64**, 094505 (1999).

[22] Y. Hatta and T. Ikeda, Phys. Rev. D **67**, 014028 (2003).

[23] J. B. Kogut *et al.*, Nucl. Phys. **B225**, 93 (1983).

[24] R.V. Gavai, S. Gupta, and R. Ray, Prog. Theor. Phys. Suppl. **153**, 270 (2004).

[25] M. D'Elia and M.-P. Lombardo, Phys. Rev. D **70**, 074509 (2004).

[26] R. V. Gavai and S. Gupta, Phys. Rev. D **65**, 094515 (2002).

[27] S. Gupta, Phys. Rev. D **64**, 034507 (2001).

[28] R. V. Gavai and S. Gupta, Phys. Rev. D **67**, 034501 (2003).

[29] R. Gupta *et al.*, Phys. Rev. D **43**, 2003 (1991).

[30] R. V. Gavai and S. Gupta, Phys. Rev. D **66**, 094510 (2002).

[31] S. Gottlieb, *et al.*, Phys. Rev. Lett. **59**, 1513 (1987).

[32] F. Karsch and E. Laermann, Phys. Rev. D **50**, 6954 (1994).

[33] C. Bernard, *et al.*, Phys. Rev. D **45**, 3854 (1992); S. Gottlieb, *et al.*, Phys. Rev. D **47**, 3619 (1993).

[34] E. Laermann, Nucl. Phys. B, Proc. Suppl. **63**, 114 (1998).

[35] M. D'Elia, A. Di Giacomo, and C. Pica, hep-lat/0408008.

[36] Preliminary exploration of this part of the QCD phase diagram may be found in J. B. Kogut and D. K. Sinclair, Phys. Rev. D **70**, 074509 (2004); hep-lat/0407041; S. Gupta, hep-lat/0202005.

[37] In [11] this downward curvature of the critical line in the $T - \mu_3$ plane is due to a lattice artifact called saturation, which occurs when each lattice site contains the maximum number of allowed fermions. This is why the downward curve has been shown dotted in Fig. 8.